Chapter 2

Combustion and Exhaust Emission Characteristics of Diesel Micro-Pilot Ignited Dual-Fuel Engine

Ulugbek Azimov, Eiji Tomita and Nobuyuki Kawahara

Additional information is available at the end of the chapter

http://dx.doi.org/10.5772/54613

1. Introduction

To satisfy increasingly strict emissions regulations, engines with alternative gaseous fuels are now widely used. Natural gas and synthesis gas appear to be greener alternatives for internal combustion engines [1-3]. In many situations where the price of petroleum fuels is high or where supplies are unreliable, the syngas, for example, can provide an economically viable solution. Syngas is produced by gasifying a solid fuel feedstock such as coal or biomass. The biomass gasification means incomplete combustion of biomass resulting in production of combustible gases. Syngas consists of about 40% combustible gases, mainly carbon monoxide (CO), hydrogen (H_2) and methane (CH_4). The rest are non-combustible gases and consists mainly of nitrogen (N_2) and carbon dioxide (CO_2). Varying proportions of CO_2, H_2O, N_2, and CH_4 may be present [4].

H_2 as a main component of a syngas has very clean burning characteristics, a high flame propagation speed and wide flammability limits. H_2 has a laminar combustion speed about eight times greater than that of natural gas, providing a reduction of combustion duration and as a result, an increase in the efficiency of internal combustion (IC) engines, if the H_2 content in the gaseous fuel increases. Main point of interest in increasing H_2 content in the gaseous fuel is that with the addition of H_2, the lean limit of the gas operation can be extended, without going into the lean misfire region. Lean mixture combustion has a great potential to achieve higher thermal efficiency and lower emissions [5]. In particular, the lean mixture combustion will result in low and even extremely low NOx levels with only a slight increase in hydrocarbons [6, 7].

Some gas engines fueled with syngas have been developed recently [8-10]. Most of them have a spark-ignition (SI) combustion system. An SI engine is not suitable for this kind of

fuel under high load conditions because of the difficulty in achieving stable combustion due to the fluctuation of the syngas components. In addition, the syngas is a low energy density fuel and the extent of power degrading is large when compared with high-energy density fuels like gasoline and natural gas. Natural gas and syngas have high auto-ignition temperature and hence cannot be used in CI engines without a means of initiating combustion, as the temperature attained at the end of the compression stroke is too low for the mixture to be auto-ignited. Therefore, dual-fuel-mode engine operation is required, in which gaseous fuel is ignited by pilot diesel fuel. Dual fueling can serve as a way of allowing the current fleet of CI engines to reduce their dependence on conventional diesel fuel while minimizing harmful emissions.

A number of researchers have performed experiments with natural gas and syngas to determine engine performance and exhaust emissions in dual-fuel engines. Their results indicate that lower NOx and smoke can be achieved in dual-fuel engines compared with conventional diesel engines, while maintaining the same thermal efficiency as a diesel engine. McTaggart-Cowan *et al.* [11] investigated the effect of high-pressure injection on a pilot-ignited, directly injected natural gas engine. They found that at high loads, higher injection pressures substantially reduce PM emissions. At low loads, the amount of PM emissions are independent of the injection pressure. Without EGR, NOx emissions are slightly increased at higher injection pressures due to the faster and more intense combustion caused by improved mixing of air and fuel and increased in-cylinder temperature. Su and Lin [12] studied the amount of pilot injection and the rich and lean boundaries of natural gas dual-fuel engines. They found that there is a critical amount of pilot diesel fuel for each load and speed. Tomita *et al.* [13] investigated the combustion characteristics and performance of the supercharged syngas with micro-pilot (injected fuel - 2 mg/cycle) ignition in a dual-fuel engine. They found that premixed flame of syngas-air mixture develops from multiple flame kernels produced by the ignition of diesel fuel. It was found that with the certain increase of hydrogen content in syngas the engine could operate even at equivalence ratio of 0.45 with stable combustion and high efficiency, because the increased hydrogen content enhanced the lean limit of the mixture. Liu and Karim [14] concluded that the observed values of the ignition delay in dual-fuel operation are strongly dependent on the type of gaseous fuels used and their concentrations in the cylinder charge. They showed that changes in the charge temperature during compression, preignition energy release, external heat transfer to the surroundings, and the contribution of residual gases appear to be the main factors responsible for controlling the length of the ignition delay of the engine.

The autoignition of the premixed mixture in the end-gas region is affected by the composition of syngas, in particular, by the amount of H_2, CO, CO_2 and CH_4 in the gas. H_2 has low ignition energy, and therefore, is easier to ignite, that results in a stronger tendency to autoignition and knock. H_2 has a flame speed much greater than that of hydrocarbon fuels. Also, it has a lean limit of ϕ_{lim}=0.1, much lower than the theoretical limit of methane (ϕ_{lim}=0.5) [15]. Carbon dioxide, on the other hand, can weaken the reactivity of the in-cylinder mixture by diluting it, which results in a longer ignition delay time and slower heat

release rate. Methane has excellent anti-knock properties, but suffers from low flame propagation rates and high auto-ignition temperature. Carbon monoxide can also affect the reactivity of the mixture. In fact, the oxidation of CO in the presence of H_2 is important question concerning the syngas oxidation mechanism. It is well known that the overall reactivity is greatly accelerated if trace amounts of H_2 and moisture are present. The oxidation route between CO and OH is the dominant pathway, and it accounts for a significant portion of the heat release [16].

The aforementioned results suggest that if certain operating conditions are maintained, including the control of pilot fuel injection quantity, pressure and timing, gaseous fuel equivalence ratio, and EGR rate, a compromise between increased efficiency and low exhaust emissions can be achieved. In this chapter, we document the range of operating conditions under which the new higher-efficiency PREMIER (**PRE**mixed **M**ixture **I**gnition in the **E**nd-gas **R**egion) combustion mode was experimentally tested. The objective of this work was in brief to discuss conventional micro-pilot injected dual-fuel combustion and in detail to explain about PREMIER combustion and emission characteristics in a pilot ignited supercharged dual-fuel engine fueled with natural gas and syngas, and to study the effect of H_2 and CO_2 content in syngas on the combustion and emission formation over the broad range of equivalence ratios under lean conditions.

2. Conventional micro-pilot injected dual-fuel combustion

2.1. Experimental procedure and conditions

This study used water-cooled four-stroke single-cylinder engine, with two intake and two exhaust valves, shown in Figure 1 (A). In this engine, the autoignition of a small quantity of diesel pilot fuel (2 mg/cycle), injected into the combustion chamber before top dead center, initiates the combustion. The burning diesel fuel then ignites the gaseous fuel. The pilot fuel was ultra low-sulfur (<10ppm) diesel. A commercial solenoid-type injector that is typically used for diesel-only operations was modified. A nozzle of the commercial injector with seven holes was replaced by the one with four holes of 0.1 mm in diameter to ensure a small quantity of injected fuel.

Diesel fuel injection timing and injection duration were controlled through the signals transferred to the injector from the injector driver. A common rail injection system (ECD U2-P, Denso Co.) was employed to supply the constant injection pressure to the injector. The common rail pressure was set and controlled via computer. The fuel injection pressure varied from 40 MPa to 150 MPa, and the injected pilot diesel fuel quantity was 2 mg/cycle and 3 mg/cycle. The experimental conditions and different types of primary gaseous fuel compositions used in this study are given in Table 1 and Table 2, respectively.

The in-cylinder pressure history of combustion cycles was measured with KISTLER-6052C pressure transducer in conjunction with a 0.5° crank-angle encoder to identify the piston location. The rate of heat release (ROHR) was calculated using this equation [17]:

$$\frac{dQ}{d\theta} = \frac{\gamma}{\gamma - 1} p \frac{dV}{d\theta} + \frac{1}{\gamma - 1} V \frac{dp}{d\theta} \tag{1}$$

where θ is the crank angle (CA), p is the in-cylinder pressure at a given crank angle, V is the cylinder volume at that point and γ is the specific heat ratio. The ROHR represents the rate of energy release from the combustion process. The combustion transition from the first stage (slow flame propagation) to the second stage (end-gas autoignition) is identified from the ROHR. CO and NOx emissions were measured with a four-component analyzer Horiba PG-240, smoke was measured with a smoke meter Horiba MEXA-600s and HC emissions were measured with Horiba MEXA-1170HFID.

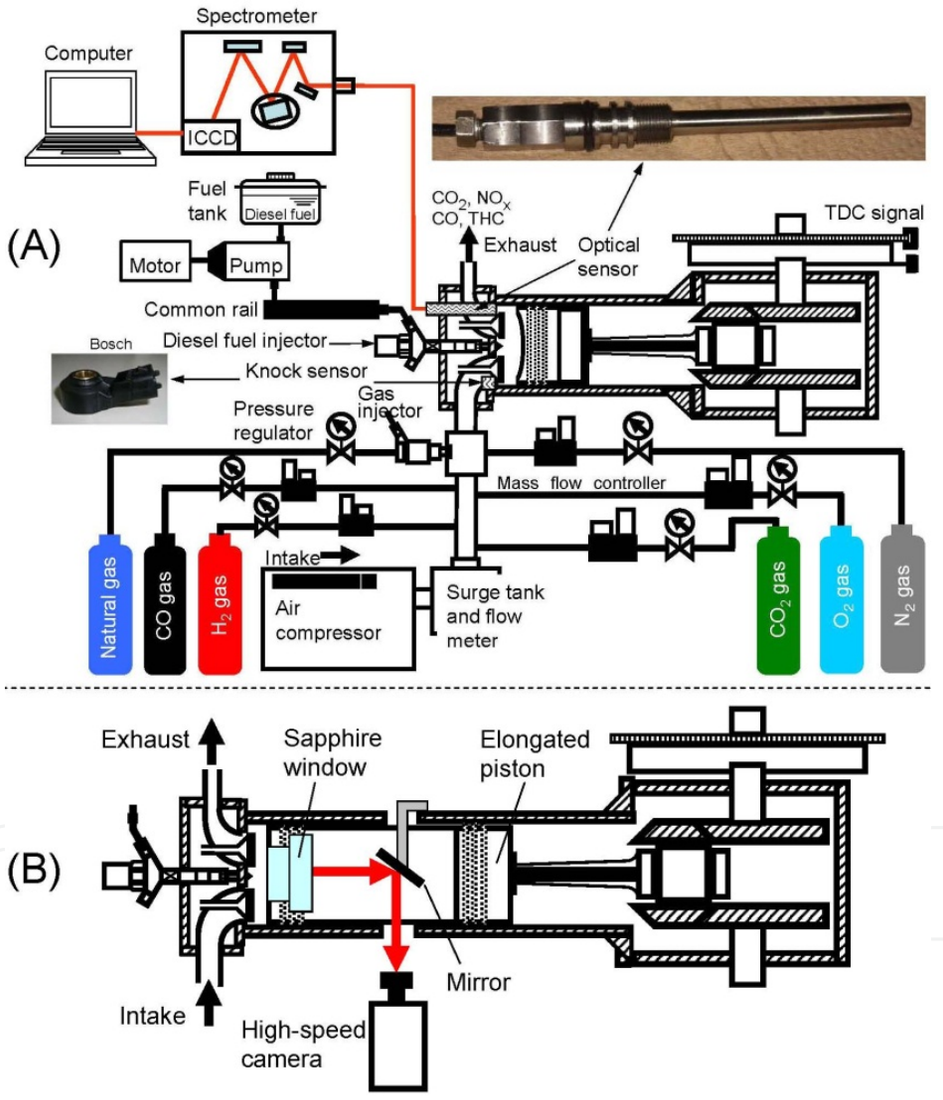

Figure 1. Experimental engine layout. (A) bench engine, (B) optical engine

An elongated cylinder liner and elongated piston were installed on the engine, Figure 1 (B), to visualize dual-fuel combustion events and to capture images of combustion in an optical engine. The engine mentioned above in Figure 1 (A) was modified to allow facilitating the visualization experiments.

Engine type	4-stroke, single cylinder, water cooled
Bore x Stroke	96x108 mm
Swept volume	781.7 cm3
Compression ratio	16
Combustion system	Dual-fuel, direct injection
Combustion chamber	Shallow dish
Engine speed	1000 rpm
Intake pressure	101 kPa, 200 kPa
Injection system	Common-rail
Pilot fuel injection pressure	
- Natural gas case	40 MPa, 80 MPa, 120 MPa, 150 MPa
- Syngas case	80 MPa
Pilot fuel injection quantity	
- Natural gas case	2 mg/cycle, 3 mg/cycle
- Syngas case	3 mg/cycle
Nozzle hole x diameter	
- Natural gas case	3x0.08 mm, 3x0.10 mm, 4x0.10 mm
- Syngas case	4x0.10 mm
Equivalence ratio	
- Natural gas case	0.6
- Syngas case	Variable
EGR rate	
- Natural gas case	10%, 20%, 30%, 40%, 50%
- Syngas case	none
EGR composition	N_2-86%, O_2-10%, CO_2-4%

Table 1. Experimental conditions

Gas type	Composition						
	H_2 (%)	CO (%)	CH_4 (%)	CO_2 (%)	N_2 (%)	LHV (MJ/kg)	Source
Type 1	13.7	22.3	1.9	16.8	45.3	4.13	BMG
Type 2	20.0	22.3	1.9	16.8	39.0	4.99	BMG
Type 3	56.8	22.3	1.9	16.8	2.2	13.64	COG
Type 4	13.7	22.3	1.9	23.0	39.1	3.98	BMG
Type 5	13.7	22.3	1.9	34.0	28.1	3.74	BMG
Type 6	56.8	5.9	29.5	2.2	5.6	38.69	COG
Type 7	56.8	29.5	5.9	2.2	5.6	20.67	COG
Type 8	100.0	-	-	-	-	119.93	Hydrogen
	CH_4 (%)	C_2H_6 (%)	C_3H_8 (%)	n-C_4H_{10} (%)		LHV (MJ/kg)	
Natural gas	88.0	6.0	4.0	2.0		49.20	

Table 2. Gas composition

A sapphire window was installed on the top of the elongated piston. Temporal and spatial evolutions of visible flames were investigated by acquiring several images per cycle with MEMRECAM fx-K5, a high speed digital camera with the frame rate of 8000 fps in combination with a 45° mirror located inside the elongated piston. An engine shaft encoder and delay generator were used to implement camera-engine synchronization. The engine was first operated with motoring, then it was fired on only one cycle during which combustion images were captured.

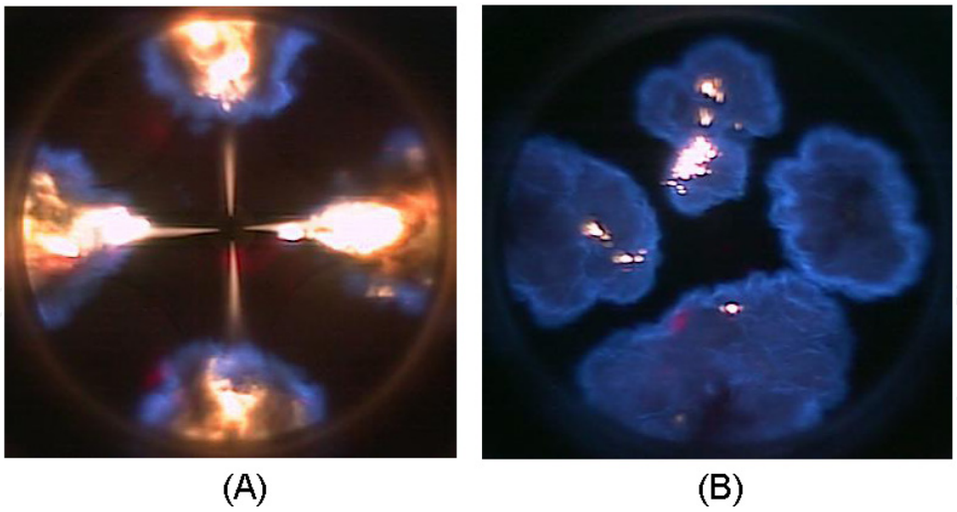

Figure 2. Dual fuel combustion of syngas with different amounts of injected diesel fuel (A) 10 mg and (B) 2 mg

Figure 2 shows the effect of pilot diesel fuel amount on combustion of syngas as a primary fuel. A distinct separation of diesel diffusion flame and syngas premixed flame is seen when larger amount of diesel fuel, 10 mg, is injected. The mixture burns only when the required oxygen is present. As a result, the flame speed is limited by the rate of diffusion. For syngas well-premixed mixture, the flame is not limited by the rate of diffusion and the mixture burning rate is much faster than that of diesel-air mixture. When only 2 mg of diesel fuel is injected the fuel evaporates and mixes with the oxidizer much faster providing distributed ignition centers in the cylinder for syngas-air mixture which is burnt as a premixed flame propagating towards the cylinder wall.

Figure 3 shows the dual-fuel combustion with natural gas (A) and syngas (B) as a primary fuel. The flame area growth for syngas is slower due to the presence of CO_2 and CO. Although syngas contains H_2, the effect of H_2 on flame propagation is not clearly seen due to simultaneous oxidation of H_2 and CO and the effect of CO_2 diluting the air-fuel mixture. The effect of CO oxidation in the presence of H_2 on flame propagation is a quite complex topic and is outside the scope of this chapter.

3. PREMIER micro-pilot ignited dual-fuel combustion

3.1. Concept of PREMIER combustion

Before giving a description to PREMIER (**PRE**mixed **M**ixture **I**gnition in the **E**nd-gas **R**egion) combustion, it is necessary to explain the differences of phenomenological outline between conventional combustion and knocking combustion in the dual-fuel engine. Conventional combustion is a combustion process which is initiated by a timed pilot ignited fuel and in which the multiple flame fronts caused by multiple ignition centers of pilot fuel, moves completely across the combustion chamber in a uniform manner at a normal velocity. Knocking combustion is a combustion process in which some part or all of the charge may be consumed (autoignited) in the end-gas region at extremely high rates. Much evidence of

end-gas mixture auto-ignition followed by knocking combustion can be obtained from high-speed laser shadowgraphs [18], high-speed Schlieren photography [19], chemiluminescent emission [20], and laser-induced fluorescence [21]. In addition, Stiebels *et al.* [22] and Pan and Sheppard [23] showed that multiple autoignition sites occur during knocking combustion. The combustion mode we have monitored we believe differs from knocking combustion in terms of the size, gradients, and spatial distribution of the exothermic centers in the end-gas. This combustion concept was given a name PREMIER combustion.

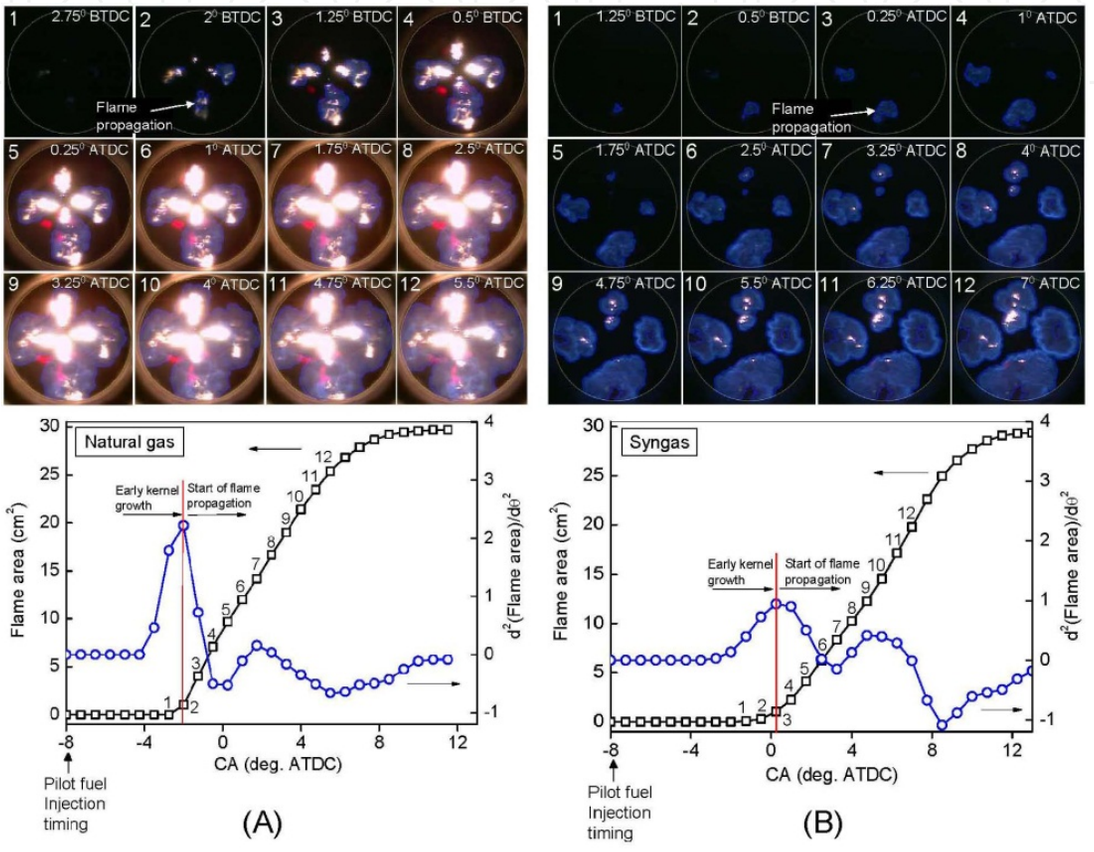

Figure 3. Dual-fuel combustion sequential images at P_{inj} = 40 MPa, P_{in} = 101 kPa, θ_{inj} = 8° BTDC, m_{df} = 2 mg/cycle, ϕ_t = 0.6. (A) natural gas, CH_4=88%, C_2H_6=6%, C_3H_8=4%, n-C_4H_{10}=2% (B) syngas, H_2=22.3%, CO=27.6%, CH_4=2.7%, CO_2=23.2%, N_2=24.2%

A conceptual outline of PREMIER combustion is presented in Figure 4. In the first stage of this combustion mode, the pilot diesel fuel is injected, evaporated, and auto-ignited prior to top dead center (TDC). The energy released by the diesel fuel auto-ignition initiates the gaseous flame development and outward propagation from the ignition centers toward the cylinder wall. Once the end-gas region is sufficiently heated and the temperature of the fuel mixture has reached the auto-ignition temperature of the gaseous fuel/air mixture after TDC, the second-stage combustion begins and is completed as the gas expands and cools, producing work. The second-stage heat release occurs over a chemical reaction timescale and is faster than heat release by turbulent flame propagation. Thus, the combustion transition from the first stage to the second stage takes place when the overall heat release rate changes from the slower first-stage flame rate to the faster second-stage rate, and that

transition is here measured as the point where the second derivative of the heat release rate is maximized, as shown in Figure 4.

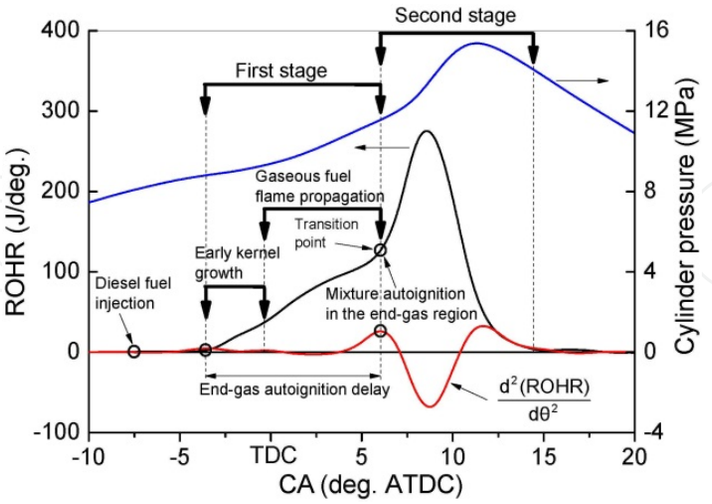

Figure 4. PREMIER combustion concept

PREMIER combustion in a dual-fuel engine is comparable to combining SI and CI combustion, which is being investigated by several researchers [24-26]. One disadvantage of these combustion strategies is that they are difficult to control under lean mixture conditions. The spark discharge is very short, and under light load and lean mixture conditions, the flame is too weak to propagate strongly and may be extinguished. Therefore, the combustion chamber must be specially designed to facilitate a stratified mixture charge around the spark plug electrodes. In a dual-fuel engine, on the other hand, combustion of the injected diesel fuel proceeds concurrently with that of the gaseous fuel mixture. This slow combustion of the diesel fuel helps to maintain the natural gas flame propagation and prevents the misfires that may occur under lean mixture conditions. The lean limit for the gaseous fuel/air mixture is of practical importance, as lean operation can result in both higher efficiency and reduced emissions. The major benefit of lean operation is the accompanying reduction in combustion temperature, which leads directly to a significant reduction in NOx emissions. The lean limit is the point where misfire becomes noticeable, and it is usually described in terms of the limiting equivalence ratio ϕ_{lim} that supports complete combustion of the mixture. For example, with the natural gas, if we operate slightly above the limiting equivalence ratio (for methane, $\phi_{lim} \approx 0.5$ [27]), the mixture reactivity becomes very sensitive to even very small variations in the air–fuel ratio. This high sensitivity is due to the presence of n-butane in the natural gas. It is known that small changes in the volume fraction of n-butane strongly affect the ignition properties of natural gas [28-31]. During hydrocarbon fuel oxidation, an H-atom is more easily abstracted from an n-butane molecule (with two secondary carbon atoms) than from other hydrocarbons such as methane, ethane, or propane [32]. As the equivalence ratio increases, the n-butane mass fraction in the natural gas/air mixture increases proportionally. During a fuel oxidation reaction, the in-cylinder gas temperature rises, and more of the radicals that initiate methane oxidation are created by increasing the ratio of n-butane. Similar results were documented

by other researchers who investigated the auto-ignition and combustion of the natural gas in an HCCI engine [33]. They found that very small increases in the equivalence ratio of the methane/n-butane/air mixture produced significant changes in the profiles of the in-cylinder pressure traces.

If not extinguished during the early combustion stage, the pilot diesel flame may continue to a later stage, and pilot flame energy contributes to the stability of the combustion process [34]. The remaining unburned in-cylinder mixture from the first stage, located beyond the boundary of the flame front, is then subjected to a combination of heat and pressure for certain duration. As the flame front propagates away from the primary ignition points, end-gas compression raises the end-gas temperature and pressure. When the mixture is preheated throughout the combustion chamber volume and the end-gas mixture reaches the auto-ignition point, simultaneous auto-ignition occurs in several limited locations (known as exothermic centers), with a sharp increase in heat release. This part of the combustion appears as a rapid energy release in the second stage of the heat release curve shown in Figure 4.

A prime requirement for maintaining PREMIER combustion mode in a dual-fuel engine is that the mixture must not auto-ignite spontaneously during or following the rapid release of pilot energy. Failure to meet this requirement can lead to the onset of knock, which manifests itself in excessively sharp pressure increases and overheating of the walls, resulting in significant loss of efficiency with increased cyclic variations. When much smaller pilots are used, the energy release during the initial stages of ignition and the resulting turbulent flame propagation can (under certain conditions) lead to auto-ignition of the charge well away from the initial ignition centers, in the end-gas regions ahead of the propagating flames. This can occur in a manner that resembles the occurrence of knock in spark-ignition engines, but with controlled heat release. For the sake of convenience, the total energy release rate during PREMIER combustion can be divided into three sequential components. The first of these is due to the ignition of the pilot fuel. The second is due to the combustion of the gaseous fuel in the immediate vicinity of the ignition centers of the pilot, with consequent flame propagation. The third is due to auto-ignition in the end-gas region.

4. PREMIER combustion detection (Natural gas)

4.1. Cyclic variations and FFT of in-cylinder pressure

Cycle-to-cycle variations of the in-cylinder pressure during conventional, PREMIER, and knocking combustion with natural gas are identified by over-plotting 80 cycles of a measured pressure trace. From Figure 5, we observe that cycle-to-cycle pressure variations were present in all cases considered, and they varied according to the injection timing θ_{inj}. It should be noted that under normal combustion conditions, the magnitude of the peak pressure (which is directly related to the power output) depends on θ_{inj}, and P_{max} is higher for advanced θ_{inj}. Unfortunately, the advantage of this peak pressure increase is offset by the disadvantages of increased fluctuation and the occurrence of knock.

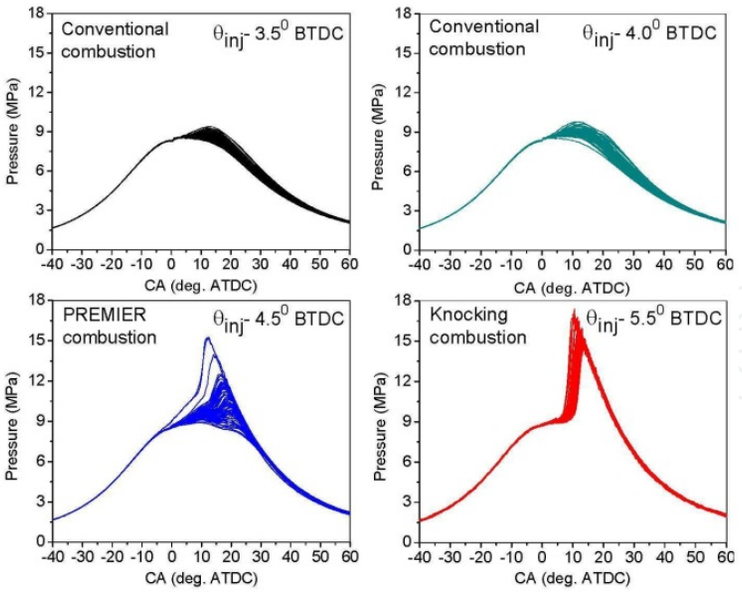

Figure 5. Cyclic maximum pressure versus its angle (Pmax, θ_{Pmax}) for different injection timings. P_{inj}=80 MPa, P_{in}=200 kPa, D_{hole}= 0.1 mm, N_{hole}=3, m_{df}=2 mg/cycle, ϕ_t=0.6

Thus, when slow combustion dominates, the P_{max} fluctuations are small, whereas during fast combustion, the P_{max} fluctuations are larger. With advanced fuel injection timing, the combustion was too fast, and the mixture auto-ignited spontaneously during or following the rapid pilot energy release. This led to the onset of knock. However, with a slight retardation of the injection timing, the energy release during the initial stages of ignition and the resulting turbulent flame propagation may induce auto-ignition of the charge in the end-gas regions ahead of the propagating flame, followed by PREMIER combustion. The stability of PREMIER combustion was confirmed by running an engine mentioned in Figure 1 (A) continuously for 30 minutes. As the engine operation reached a steady condition, P_{max} stabilized within a definite range between conventional and knocking combustion modes. It should be noticed that the present achieved stability of PREMIER combustion allows using this mode in stationary engines, such as engines used for power generation. In order to utilize PREMIER combustion in vehicles, further research is required to find optimum ways to precisely control the conditions inside the cylinder at various loads.

The transition from PREMIER combustion to knocking combustion was evaluated by fast Fourier transform (FFT) analysis of the in-cylinder pressure and the knock-sensor signal. The details of FFT analysis are given in [35]. Unlike during knocking in traditional spark-ignition engines, high frequency oscillations of in-cylinder pressure and knock-sensor signals were not observed during the PREMIER combustion mode.

The in-cylinder pressure and knock-sensor signals were filtered using an FFT band-pass filter with 4-20 kHz cutoff frequencies. The filtered pressure data was used to define the knock intensity. Figure 6 shows that during PREMIER combustion mode, the measured cylinder pressure curve was smooth, and the maximum rate of pressure rise (which was only 0.36 MPa/CA deg.) occurred at 17° ATDC under the conditions P_{int}=200 kPa, m_{df}=2 mg/cycle, P_{inj}=80 MPa and θ_{inj}=4.5° BTDC. Pressure oscillations did not occur, and the

pressure sensor was unable to detect a sawtooth pattern on the measured pressure trace. For the same conditions mentioned above, but at $\theta_{inj}=5^{\circ}$ BTDC, the transition from PREMIER to knocking combustion occurred at the maximum rate of pressure increase ($dP/d\theta=0.55$ MPa/CA deg.), with a knock intensity of $K_{INT}=0.3$ MPa. At $\theta_{inj}=5.5^{\circ}$ BTDC, strong knocking combustion was detected with $dP/d\theta=1.87$ MPa/CA deg. and $K_{INT}=1.45$ MPa. As the figure indicates, oscillations of the in-cylinder pressure and the knock sensor signal were not detected during PREMIER combustion mode. Weak oscillations were detected during the transition from PREMIER to knocking combustion, and stronger oscillations were detected at 6.52 kHz and 10.1 kHz during knocking combustion. The peak at the transition to knocking combustion was correspondingly lower than the peak that occurred during heavy knocking combustion.

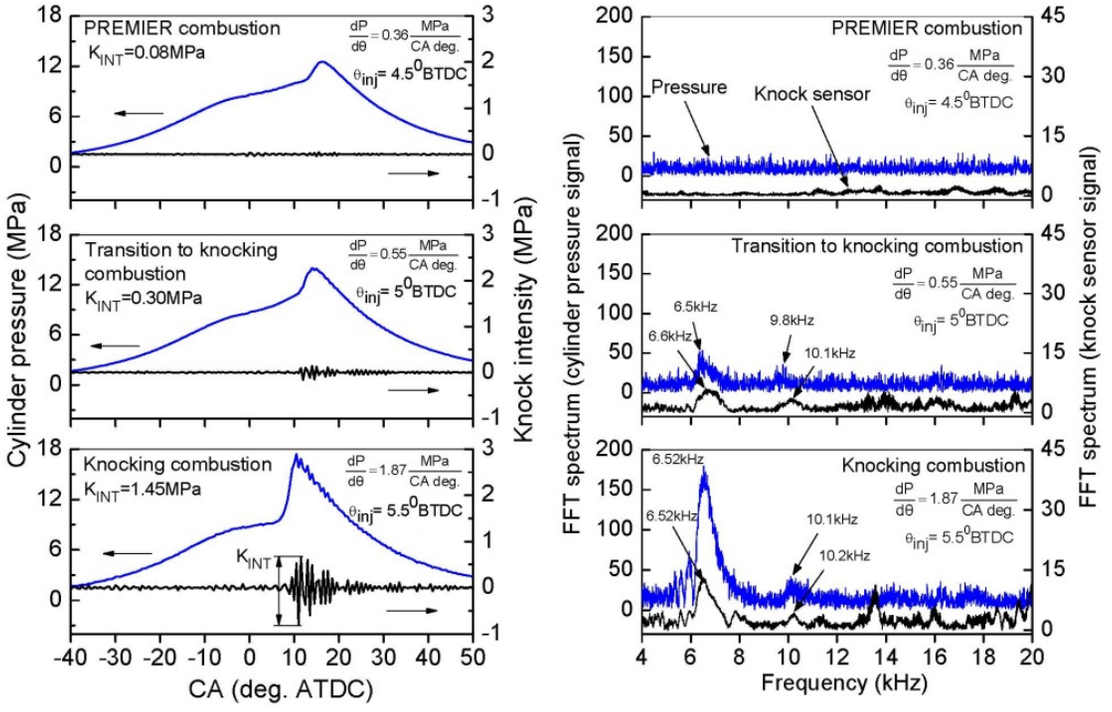

Figure 6. FFT analysis of in-cylinder pressure. $P_{inj}=80$ MPa, $P_{in}=200$ kPa, $D_{hole}=0.1$ mm, $N_{hole}=3$, $m_{df}=2$ mg/cycle, $\phi_t=0.6$

4.2. Spectroscopy analysis

The configuration of our optical engine made it difficult to directly visualize auto-ignition in the end-gas region with an optical engine setup shown in Figure 1 (B). Since auto-ignition in the end-gas region usually occurs closer to the cylinder wall, the auto-ignition region was hidden from the camera view by the top of the elongated piston, where a sapphire window was installed. Thus, an optical sensor was inserted in the region based on the most probable occurrence of auto-ignition in the end-gas region, as shown in Figure 7. The small effect of measurement location on autoignition and flame development was confirmed based on several preliminary experiments. Besides, this measurement location was selected to keep the sensor away from the highly luminescent soot radiation. If the sensor is placed too close

to the luminous emissions from diesel combustion, these emissions can supersede the OH* radical emissions, which are expected to occur during PREMIER combustion. Chemical luminescence emissions from the propagating flame and end-gas region auto-ignition were measured using a spectrometer equipped with intensified charge-coupled device (ICCD). The regions of spectroscopy measurements for conventional, PREMIER and knocking combustion, along the crank angle degrees, are shown in Figure 8. In-cylinder pressure and the rate of pressure rise change as injection timing is advanced for conventional, θ_{inj}=4° BTDC, PREMIER, θ_{inj}=8° BTDC and knocking, θ_{inj}=13° BTDC, combustion. Exposure time of the spectrometer for all three combustion regimes was set to 3° CA. The highlighted region on each graph shows the interval within which the measurements were taken.

Figure 9 shows the background light-subtracted ensemble-averaged spectra obtained between 200 and 800 nm as the propagating flame arrived in the vicinity of the optical sensor and auto-ignition occurred in the end-gas region. The background light was subtracted by the signal processing using a percentile filter. The waveforms of the emission spectroscopy were obtained for knocking cycles in the range of 0°-3°, 3°-6°, and 6°-9° ATDC, for PREMIER cycles in the range of 6°-9°, 9°-12°, and 12°-15° ATDC, and for conventional cycles in the range of 12°-15°, 15°-18°, and 18°-21° ATDC.

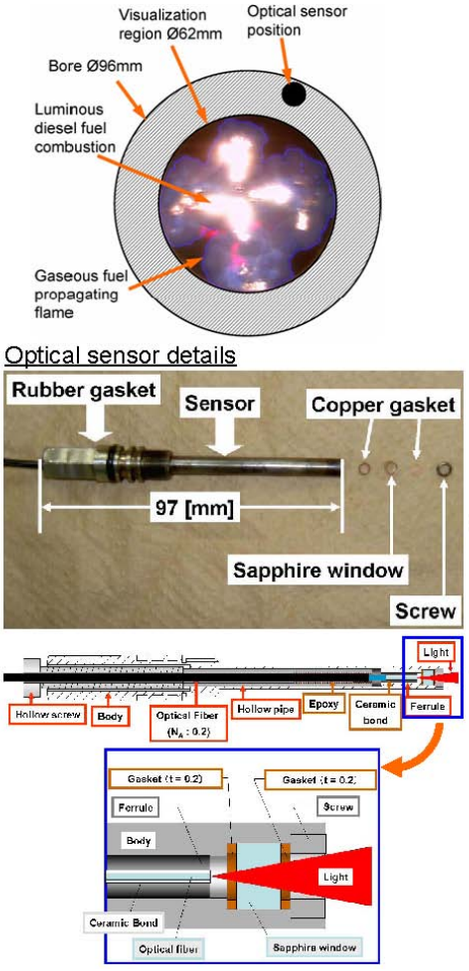

Figure 7. Optical sensor location and design

High OH* radical emission intensities were evident at wavelength 310 nm and very weak intensities at wavelength 286 nm when the flame front reached the optical sensor location region. OH* radical emission intensities at this wavelengths were stronger for knocking combustion cycles than for PREMIER combustion cycles, and for conventional combustion cycles these emission intensities were not seen. A similar trend was observed by Itoh *et al.* [36] and Hashimoto *et al.* [37]. These authors reported that under non-knocking operation, OH* radicals exhibit comparatively weak emission intensities. However, the OH* radical emission intensity gradually increased for autoignition and knocking cycles in comparison with a conventional cycle.

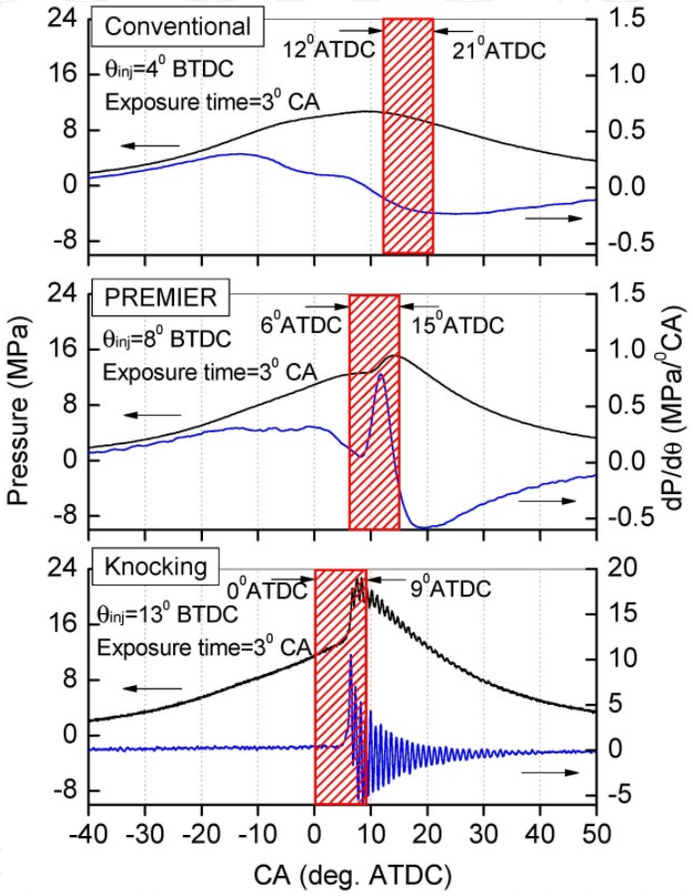

Figure 8. In-cylinder pressure and the rate of pressure rise. P_{inj}=40 MPa, P_{in}=200 kPa, D_{hole}=0.1mm, N_{hole}=3, m_{df}=2 mg/cycle, ϕ_t=0.6

Figure 9 shows that for the knocking cycle, the OH* peak at 310 nm increased sharply at 6° ATDC and then decreased at 9° ATDC. 6° ATDC corresponds to the timing of the maximum rate of pressure rise, and 9° ATDC corresponds to the timing when the rate of pressure rise is gradually decreased. Before natural gas propagating flame (1st stage combustion) is stabilized, the rapid autoignition occurs in multiple spots. The end-gas autoignition kernel growth rate is much faster than that of flame propagation.

The drastic increase in OH* emissions is related to the sharp pressure and temperature increases in the end-gas region. It has been reported that the concentration of OH* radicals

shows a strong temperature dependence in the thermal ignition region [38]. The thermal ignition is the hydrogen-oxygen system reactions, and the CO conversion into CO_2 with the assistance of OH* takes place simultaneously with the hydrogen-oxygen system reactions. It has been observed that the OH* emission intensity at auto-ignition shows the same tendency as the correlation between the occurrence of auto-ignition and the knocking intensity [39]. On the other hand, the OH* peaks of PREMIER combustion at 12° and 15° ATDC have the same magnitude. 12° ATDC corresponds to the timing of the maximum rate of pressure rise, and 15° ATDC corresponds to the timing after the peak of the rate of pressure rise. The reason for the same magnitude in OH* is that the maximum rate of pressure rise is slower than that of during knocking case. The end-gas autoignition kernel growth rate is comparable with that of flame propagation. The mixture in the end-gas region reacts steadily with the steady OH*emission.

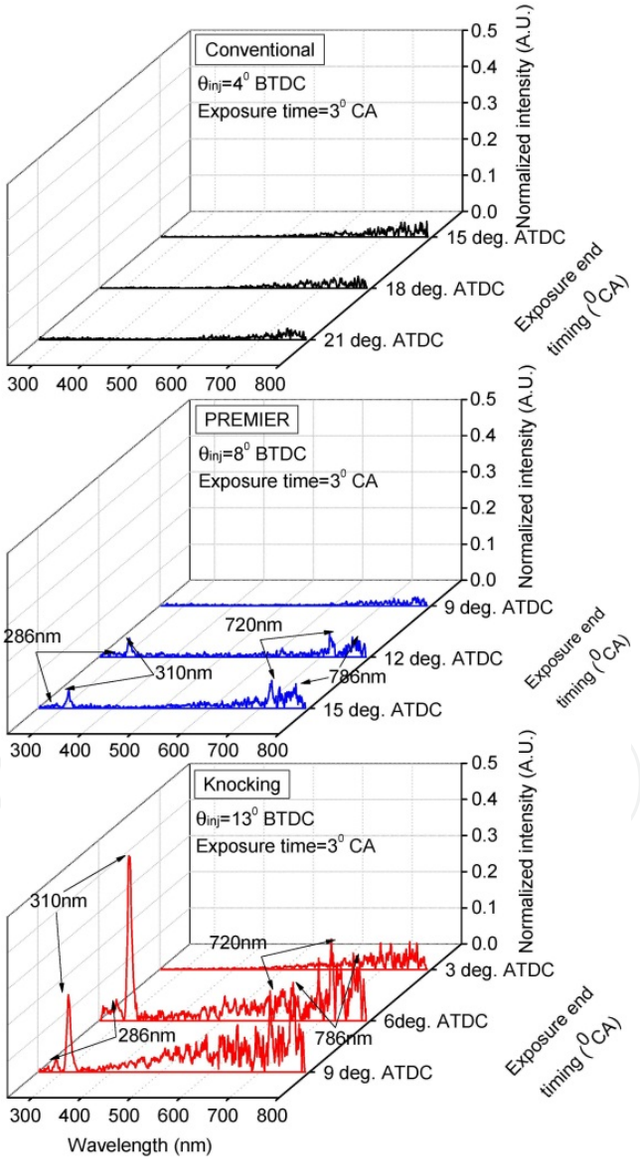

Figure 9. Detailed spectra in the end-gas region. P_{inj}=40 MPa, P_{in}=200 kPa, D_{hole}=0.1 mm, N_{hole}=3, m_{df}=2 mg/cycle, ϕ_t=0.6

The emissions at the wavelengths above 700 nm are due to diesel luminous flame. The previous shock tube measurements showed that continuum emission at wavelengths above 650 nm was due to either young soot particles or large hydrocarbon molecules [40]. Zhao and Ladommatos [41] showed that the maximum emissive power of soot particles, estimated as a blackbody, occurs in the range of about 680–1100 nm. Vattulainen *et al.* [42] confirmed that the light emitted by a diesel flame is dominated by soot incandescence, and the emission range was determined to be about 650–800 nm. The emissions at the wavelengths above 700 nm shown in Figure 9 correspond to 1-5% of the total wavelength emission band from a blackbody at the estimated average peak burned-gas temperature of 2310 K under knocking conditions, which correspond to 1.823×10^5-4.935×10^5 W/m^2·μm of spectral emissive power, with the maximum spectral emissive power at that temperature that equals to 8.459×105 W/m^2·μm [43].

5. PREMIER combustion characteristics

5.1. Natural gas combustion characteristics

To maintain PREMIER combustion in a dual-fuel natural gas engine, the effects of several operating parameters must be identified. Our experimental results show that the major parameters that may significantly influence the energy release pattern during dual-fuel PREMIER combustion are pilot diesel fuel injection timing and the EGR rate, which can affect the total equivalence ratio based on oxygen content. Other parameters such as pilot fuel injection pressure, injected pilot fuel amount, nozzle hole diameter, and hole number have minor effects on PREMIER combustion.

5.1.1. Effect of injection timing

As shown in Figure 10, PREMIER combustion can be maintained within a wide range of pilot fuel injection pressures. However, it can be maintained within only a very narrow range of fuel injection timings. At a fixed total equivalence ratio, advancing the injection timing resulted in the earlier occurrence of combustion during the cycle, increasing the peak cylinder pressure during first-stage combustion. With the burned gas of first-stage combustion, the in-cylinder pressure and temperature continued to rise after TDC, as shown in Figure 10. Although the piston began to move downward after TDC, and the volume thus expanded, the heat release from first-stage combustion induced local temperature and pressure increases during second-stage combustion. Higher peak cylinder pressures resulted in higher peak charge temperatures. Retarding the injection timing decreased the peak cylinder pressure during first-stage combustion, as more of the fuel burned after TDC.

Advancing the injection timing resulted in better diesel fuel evaporation and mixing with the in-cylinder gas. Therefore, diesel fuel auto-ignition occurred more quickly and with more complete diesel fuel combustion and natural gas flame propagation during the first stage, resulting in rapid combustion and high heat release rate during the second stage due to the rapid heating of the end-gas region mixture.

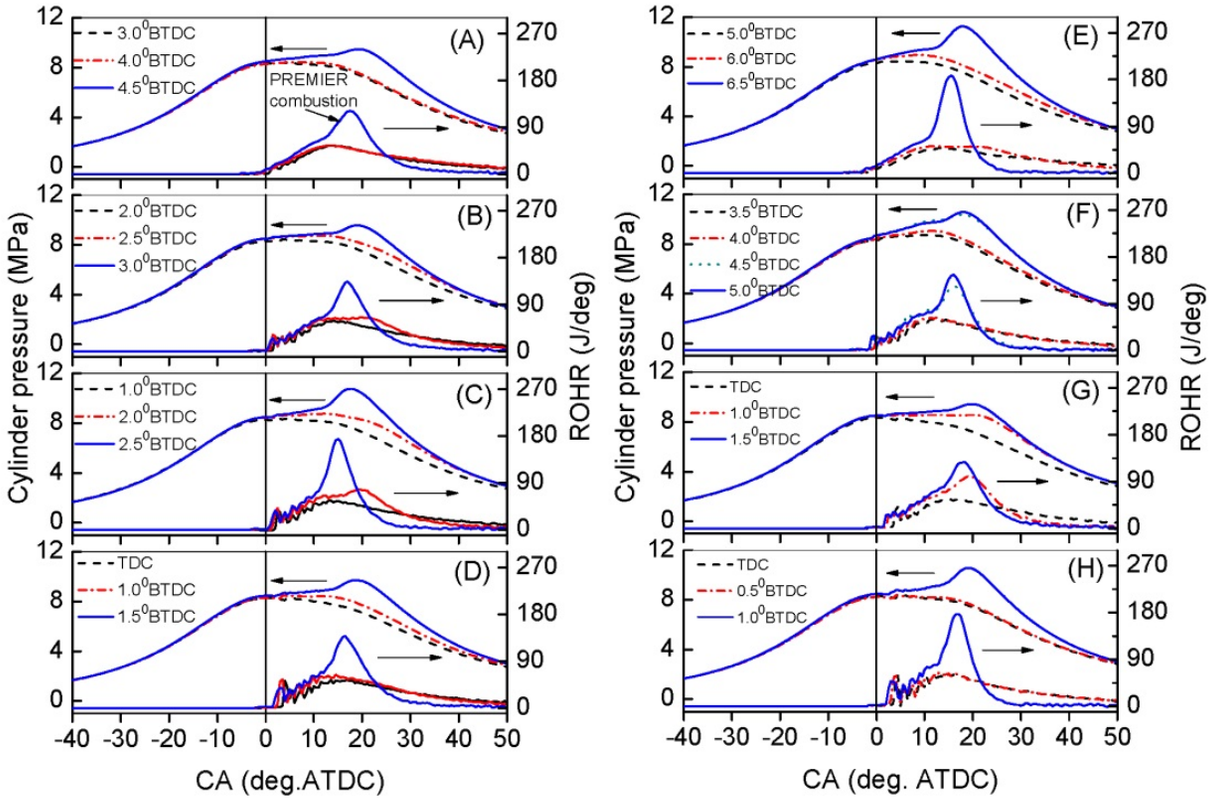

Figure 10. Effect of pilot fuel injection timing on cylinder pressure and the rate of heat release. Experimental conditions are given in Table 3.

	Injection pressure P_{inj} (MPa)	Intake pressure P_{in} (kPa)	Nozzle hole diameter D_{hole} (mm)	Nozzle hole number N_{hole}	Injected pilot fuel amount m_{df} (mg/cycle)
A	40	200	0.1	3	3
B	80	200	0.1	3	3
C	120	200	0.1	3	3
D	150	200	0.1	3	3
E	40	200	0.1	3	2
F	80	200	0.1	3	2
G	150	200	0.08	3	3
H	150	200	0.1	4	3

Table 3. Experimental conditions for Figure 10

5.1.2. Mass fraction burned in the second stage of ROHR

Figure 11 shows a relation between the rate of maximum pressure rise and the second stage autoignition delay. The second stage autoignition delay time was estimated as a time between two peaks of the second derivative of the ROHR, as shown in Figure 4. Figure 11 also shows that for the range of experimental conditions the mass fraction burned during the second stage of the ROHR is remained nearly the same, although IMEP increases. This increase in IMEP is due to faster and more intense combustion with the shorter duration in both first and second stage of the ROHR. Reduced heat loss during shorter combustion

duration ensures higher in-cylinder pressure and temperature, and therefore, higher IMEP. This trend suggests that the second stage combustion is influenced by the first stage. Although the mass fraction burned in the second stage is the same, the combination of several operational parameters such as pilot fuel injection pressure, injection timing, the amount of injected pilot fuel, gaseous fuel equivalence ratio and nozzle characteristics may affect, to a certain degree, the progress of PREMIER combustion.

	P_{inj} (MPa)	θ_{inj} (°BTDC)	m_{df} (mg/cycle)	D_{hole} (mm)	N_{hole}
1	150	1	3	0.08	3
2	80	3	3	0.1	3
3	150	1.5	3	0.08	3
4	120	2.5	3	0.1	3
5	40	4.5	3	0.1	3
6	80	5	2	0.1	3
7	80	4.5	2	0.1	3
8	150	1	3	0.1	4
9	150	1.5	3	0.1	3

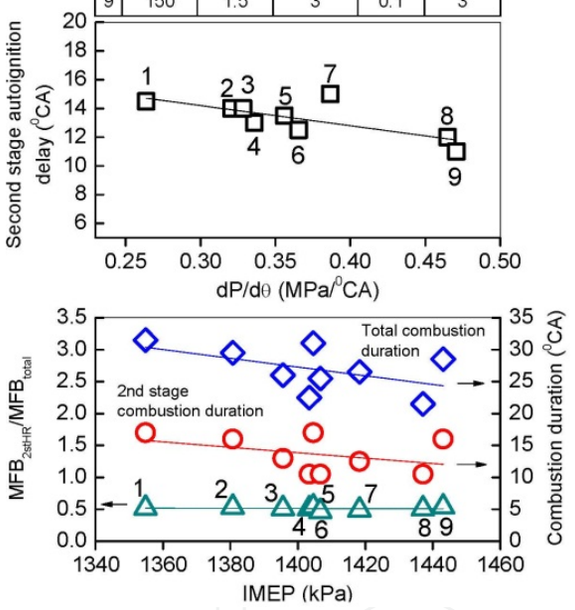

Figure 11. Second stage autoignition delay and mass fraction burned during the second stage of combustion of natural gas

5.1.3. Effect of EGR

PREMIER combustion becomes clearly recognizable if the EGR rate remains below a certain level. When the EGR rate surpasses this level, the unburned mixture temperature decreases, retarding the combustion of the natural gas and affecting the reactivity of the mixture to auto-ignite in the end-gas region. As Figure 12 shows, at 200 kPa of intake pressure and moderate EGR rates, the first-stage combustion rate increased, and second-stage heat release was able to occur. A similar trend was also observed at 101 kPa of intake pressure, although not shown here. These results suggest that the use of EGR may not be advantageous for achieving PREMIER combustion. However, it should be noted that for engine operation close to the knock-limit conditions, the high combustion rate of natural gas may be

markedly decreased by using a certain limited EGR rate, and maintaining PREMIER combustion mode as the knocking effect is suppressed.

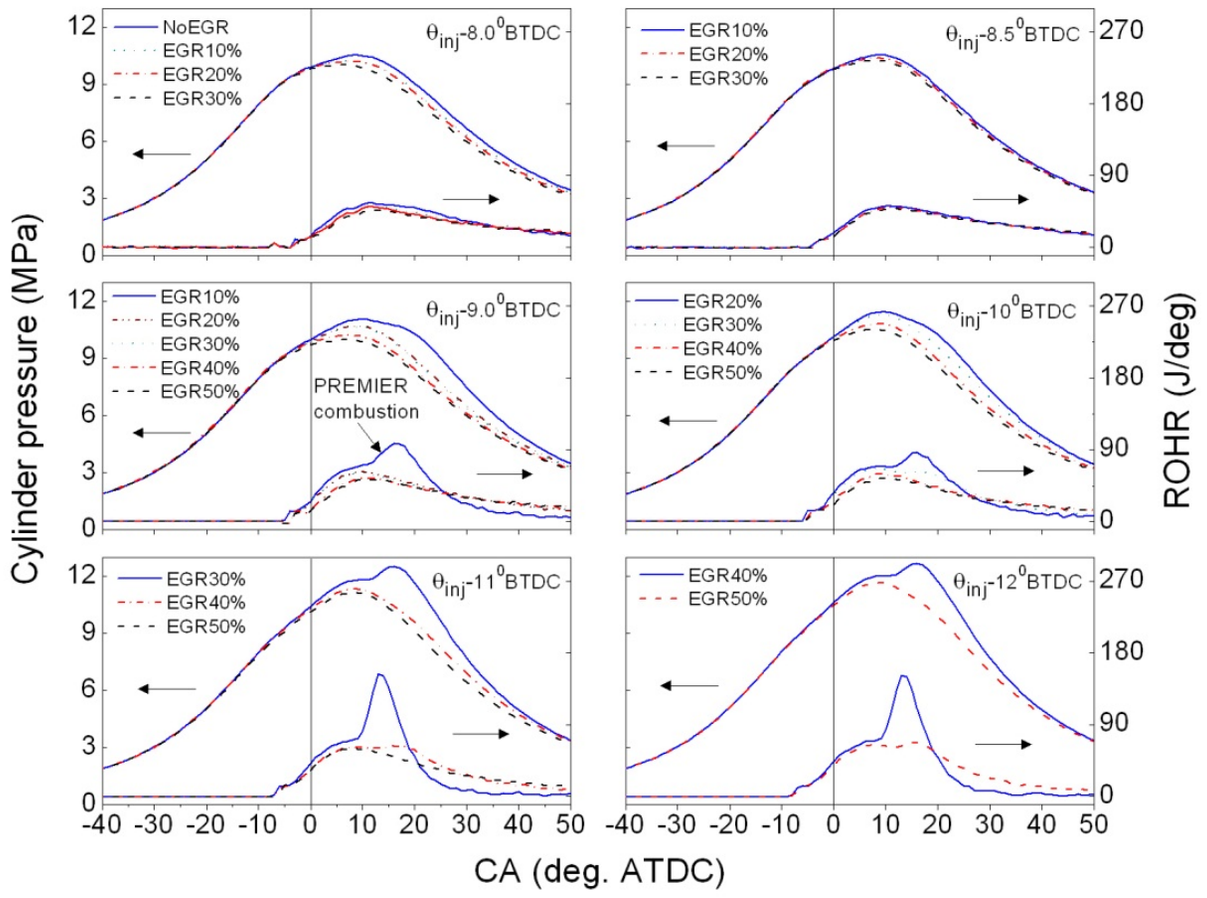

Figure 12. Effect of EGR on cylinder pressure and the rate of heat release. P_{inj}=40 MPa, P_{in}=200 kPa, D_{hole}=0.1 mm, N_{hole}=3, m_{df}=2 mg/cycle

5.2. Natural gas exhaust emission characteristics

Figure 13 shows the engine performance characteristics and exhaust gas emissions. The encircled data on (A) and (B) of the figure correspond to PREMIER combustion. During PREMIER combustion, a considerable increase in the indicated mean effective pressure and thermal efficiency was observed. This was due to the sharp increase of the second heat-release peak within a shorter crank-angle time, as seen in Figures 10 and 12. Moreover, this implies that the total combustion time for PREMIER combustion mode was shorter than the total time required for conventional combustion. Although HC and CO emissions were greatly decreased, NOx emissions increased considerably compared with conventional combustion. This increase in NOx emissions is expected, as in-cylinder temperature increase hastens the oxidation reactions of in-cylinder nitrogen and oxygen.

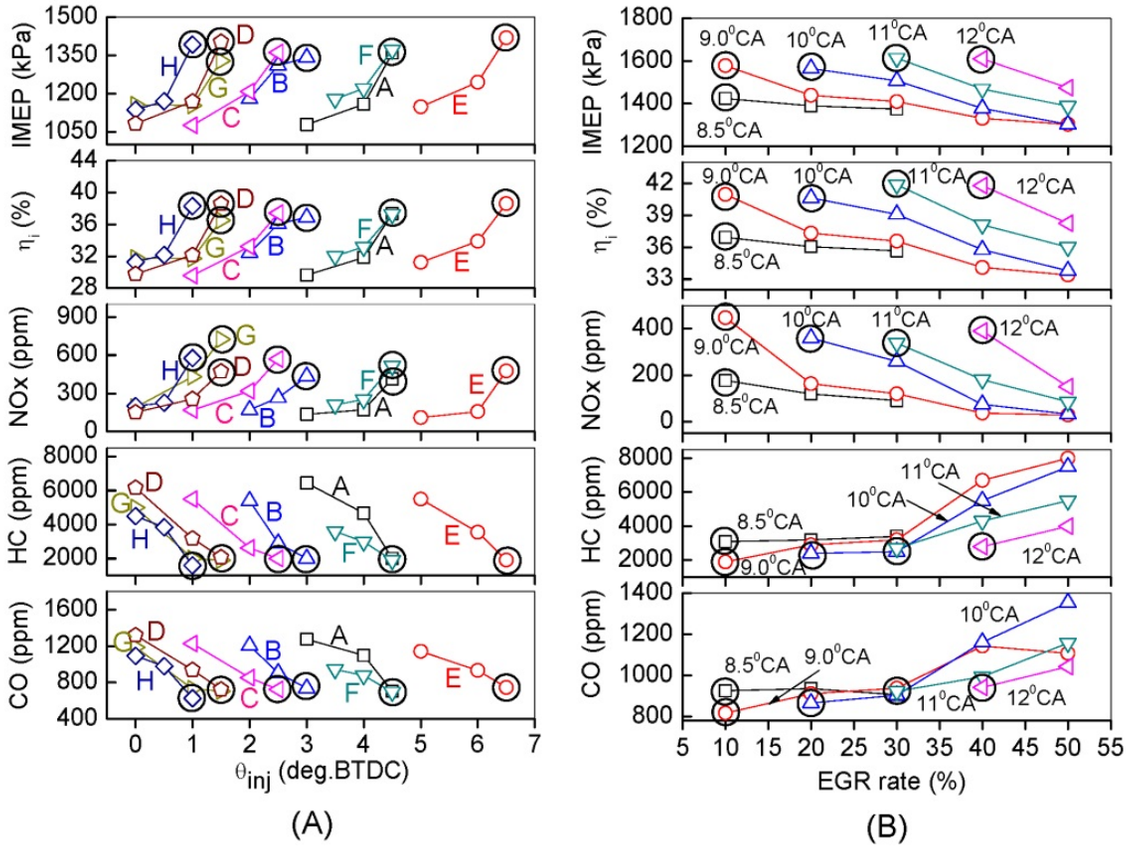

Figure 13. Effect of pilot fuel injection timing and EGR on engine performance and emissions. (A) conditions correspond to those of Figure 10, (B) conditions correspond to those of Figure 12.

5.3. Syngas combustion characteristics

Figure 14 indicates the relationship between the rate of maximum pressure rise and the second stage autoignition delay. The second stage autoignition delay time was estimated as time between two peaks of the second derivative of the ROHR as shown in Figure 4. It was found that for all types of gases investigated in this chapter the autoignition delay of the second stage decreases with the increase of the rate of maximum pressure rise.

Figure 15 shows the in-cylinder pressure and ROHR for Type 1 (A) and Type 2 (B) of syngas at different equivalence ratios and various injection timings. The results show that the maximum pressure and heat release rate reached higher values for the gas with higher H_2 content. As the injection timing was gradually advanced, PREMIER combustion with second-stage heat release occurred. PREMIER combustion was observed at various equivalence ratios for certain injection timings. For instance, for Type 1 gas, two-stage heat release appeared at $\phi = 0.4$ starting from 23° BTDC, at $\phi = 0.52$ from 15° BTDC, at $\phi = 0.68$ from 9° BTDC, and at $\phi = 0.85$ from 7° BTDC. The same trend was observed for Type 2 gas, but the maximum heat release rate was higher than that of Type 1, due to the higher H_2 content. The maximum cylinder pressure for Type 2 decreased at an equivalence ratio of 0.83, since the injection timing in that case needed to be retarded to around TDC (and even to the expansion stroke) to avoid knock. At the same time, for Type 1 gas at an equivalence ratio of

0.85 and injection timings before TDC, PREMIER combustion was clearly observed without any knock. These results seem to suggest that the increased H_2 content of Type 2 gas affected the ignitability and corresponding progress of combustion that leads to engine knock.

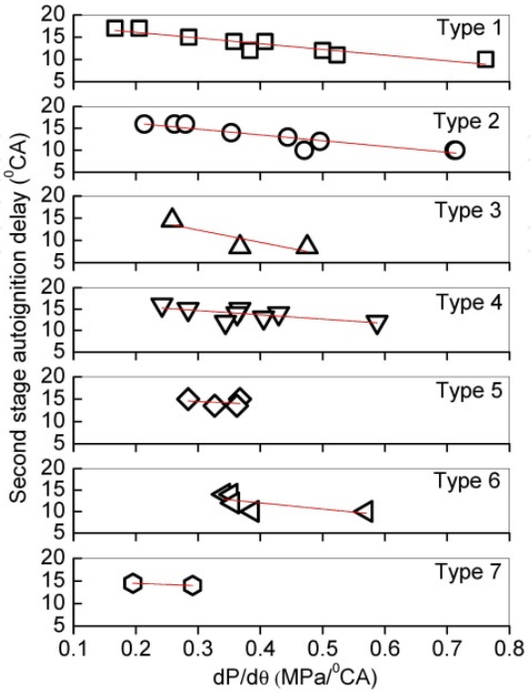

Figure 14. Second stage autoignition delay. P_{inj}=80 MPa, P_{in}=200 kPa, m_{df}=3 mg/cycle

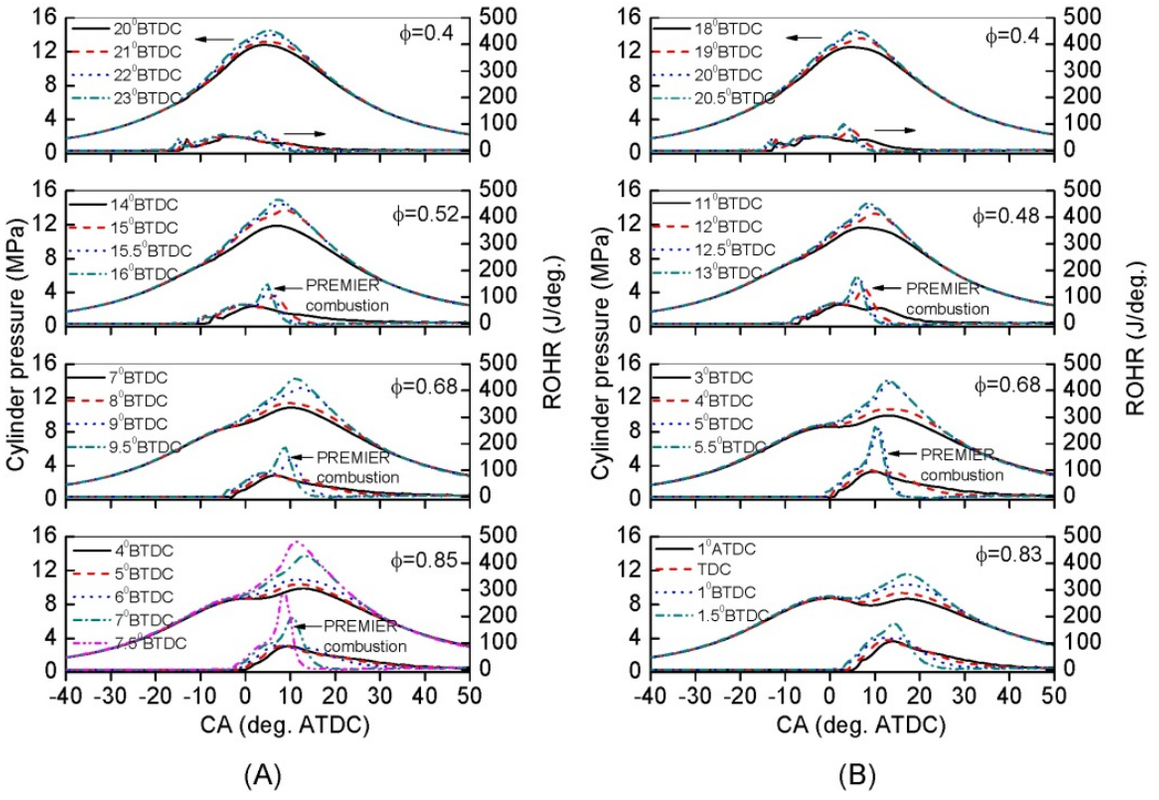

Figure 15. Comparison of in-cylinder pressure and ROHR. Syngas, (A) Type 1, (B) Type 2

5.3.1. Effect of H_2 content on PREMIER combustion

An increase in hydrogen content of syngas results in an increase of ignitability and a corresponding reduction in ignition delay of the first stage. To investigate the effect of mass fraction burned in the second stage and the effect of hydrogen content on the rate of maximum pressure rise, the ratio MFB_{2stHR}/MFB_{total} was evaluated. MFB_{2stHR} is the integral of the mass fraction burned during the second stage, computed from the transition point where the peak of $d^2(ROHR)/d\theta^2$ is maximized to the 80% MFB. MFB_{total} is the integral of the total mass fraction burned, computed from the first peak of $d^2(ROHR)/d\theta^2$ to the 80% MFB. Figure 16 shows that as the mass fraction burned increases the rate of maximum pressure rise also increases. The same trend was monitored at various equivalence ratios.

Figure 17 shows the effect of H_2 content on the mean combustion temperature, IMEP, indicated thermal efficiency and NOx for conventional and PREMIER combustion at the same input energy Q_{in}=2300 J/cycle and injection timing at the minimum advance for the best torque (MBT). As this figure shows, the increase in H_2 amount affects the engine combustion characteristics. For PREMIER combustion, the mean combustion temperature and consequently the NOx significantly increase when compared with those of conventional combustion. IMEP and indicated thermal efficiency increase about 10%. Therefore, in dual-fuel combustion of low-energy density syngas, PREMIER combustion is an important combustion mode that tends to increase the engine efficiency.

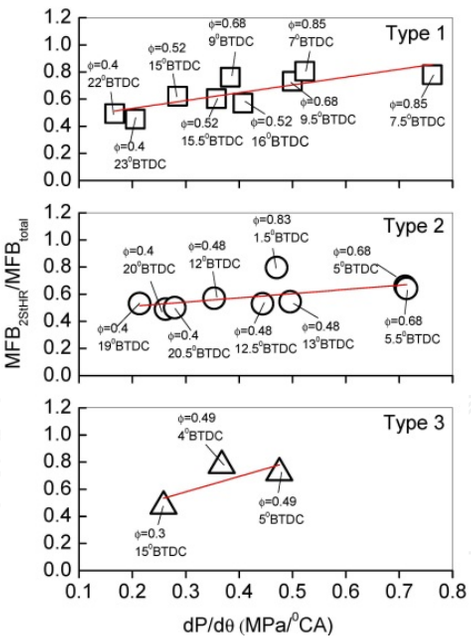

Figure 16. Fuel mass fraction burned with the change of H_2 content

5.3.2. Effect of CO_2 content on PREMIER combustion

An increase in CO_2 content in syngas results in a dilution of the mixture with the corresponding reduction in the rate of fuel oxidation reactions and consequent combustion. To investigate the effect of mass fraction burned in the second stage and the effect of CO_2

content on the rate of maximum pressure rise, the same procedure was applied as explained in the previous section.

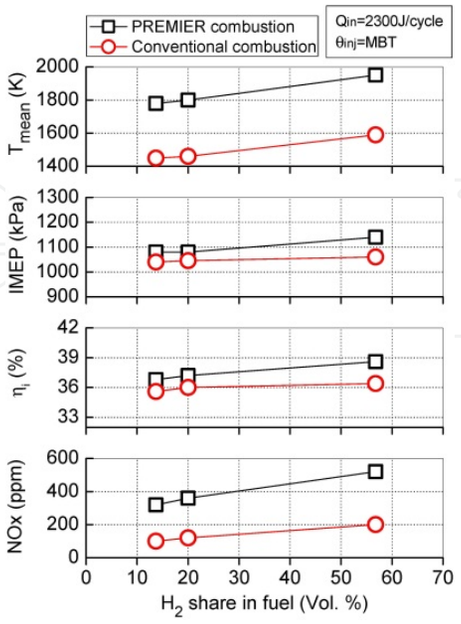

Figure 17. Effect of H_2 content on engine performance characteristics at θ_{inj}=MBT

Figure 18 shows that for Type 1 and Type 4 as the mass fraction burned during the second stage increases the rate of maximum pressure rise also increases. However, for Type 5 with 34% of CO_2 content in syngas, the rate of maximum pressure rise decreases with the increase of the mass of fuel burned in the second stage. This can be explained by the fact that although the total mass of syngas burned during the second stage increases, the CO_2 fraction in the gas also proportionally increases. Eventually, the certain threshold can be reached when the effect of CO_2 mass fraction in the gas on combustion overweighs the effect of H_2.

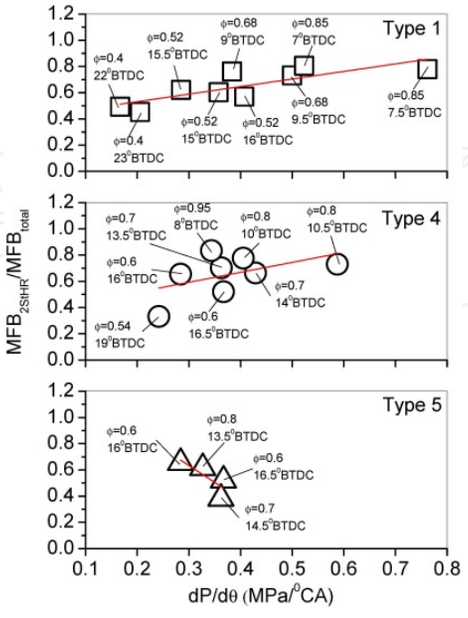

Figure 18. Fuel mass fraction burned with the change of CO_2 content

Figure 19 shows the effect of CO_2 content on the mean combustion temperature, IMEP, indicated thermal efficiency and NOx for conventional and PREMIER combustion at the same input energy Q_{in}=2300 J/cycle and injection timing at MBT. In this figure the trend mentioned earlier in Figure 18 is clearly observed.

The mean combustion temperature, IMEP, the indicated thermal efficiency and the NOx shows the increase when CO_2 content in the gas increases from 16.8% to 23%. However, as CO_2 concentration reaches 34%, above mentioned combustion characteristics decrease. This trend was observed for both conventional and PREMIER combustion. Therefore, in order to achieve high combustion efficiencies in dual-fuel engines fuelled with low-energy density syngas, CO_2 fraction in syngas needs to be controlled.

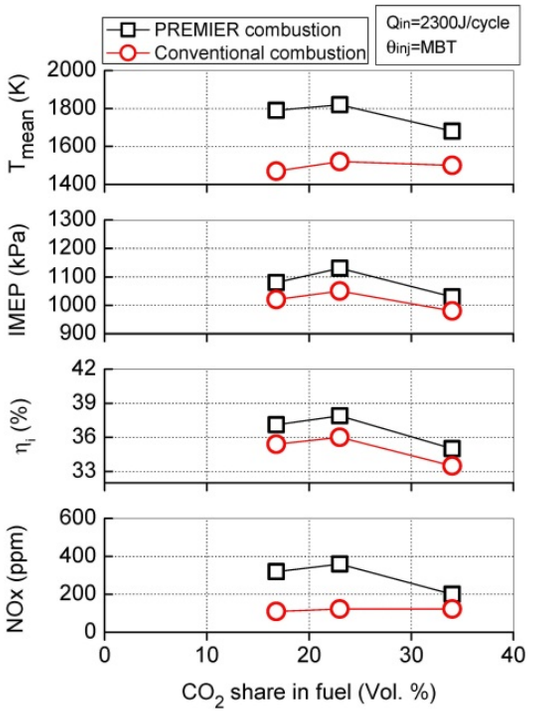

Figure 19. Effect of CO_2 content on engine performance characteristics at θ_{inj}=MBT

5.4. Syngas exhaust emission characteristics

Increasing hydrogen content in syngas has a substantial impact on engine performance and pollutants formation. Engine performance characteristics and concentrations of pollutants CO, HC and NOx are shown in Figures 20 and 21. It should be noticed that the smoke level was negligibly low. Figure 3 (B) shows highly luminous diesel fuel droplets burn exposed to the high temperature syngas flame. This concurrent micro-pilot diesel fuel and syngas combustion contributes to the faster oxidation and burn out of soot by the end of the combustion process.

Figures 20 and 21 show the experimental operation region for IMEP, CO, HC and NOx. The comparison is given for H_2 effect between Type 1 and Type 2, for CO_2 effect between Type 1 and Type 5, and for gas - type effect between Type 6 (Coke-oven gas) and Type 8 (Pure

hydrogen). The dash-dotted line is the boundary separated the conventional combustion from the PREMIER combustion at corresponding equivalence ratios and injection timings.

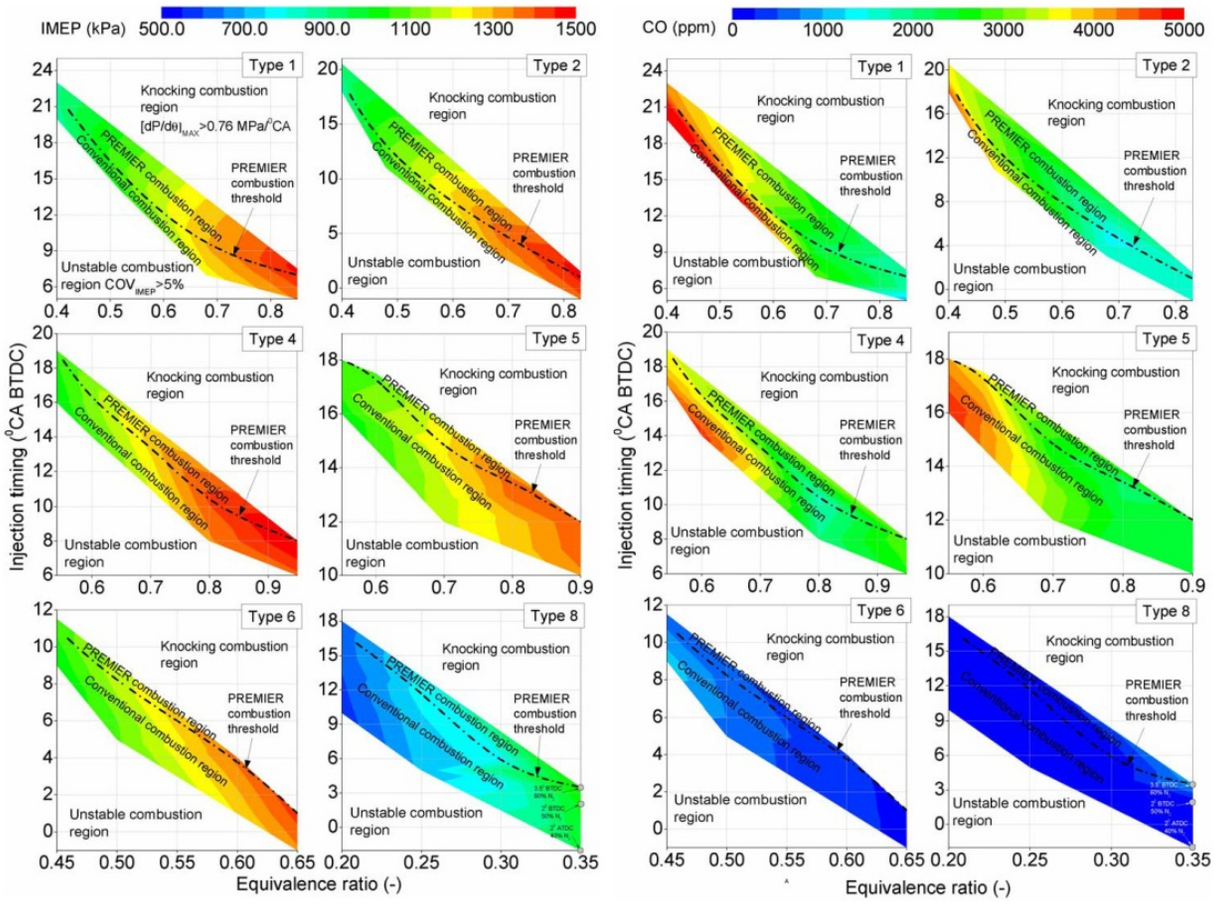

Figure 20. Experimental mapping of IMEP and CO distribution

Figure 20 shows that higher IMEP levels appear at higher equivalence ratios and advanced injection timings. PREMIER combustion mode may pass through different IMEP levels, depending on the equivalence ratio and injection timing. As H_2 fraction increases in the syngas (from Type 1 to Type 2), PREMIER combustion region expands at lower equivalence ratios and shrinks at higher equivalence ratios. On the contrary, as CO_2 fraction increases in the syngas, from Type 1 (16.8% CO_2) to Type 5 (34% CO_2), the same maximum level of IMEP, as for Type 1 and 2, can be achieved with only higher equivalence ratios. Type 1 and Type 5 show that as CO_2 content increases IMEP slightly decreases. With the increase of CO_2 fraction in the syngas the PREMIER combustion region threshold is shifted towards the boundary of operation domain. This implies that the operational region of PREMIER combustion mode is reduced.

Figure 20 (Type 1 and Type 2) and Figure 21 (Type 1 and Type 2) show that with the increase of H_2 concentration in the gas content, CO and HC emissions are reduced. The cause of these reductions is most likely the enhanced oxidation occurring because of improved combustion and higher concentrations of reactive radicals since the carbon

content in the gas is the same for both types of fuel. The NOx emissions, as in Figure 21, are higher for Type 2 than those for Type 1 due to higher H_2 content. This is in part a direct result of hydrogen's higher flame temperature effect on NO formation chemistry. NOx emissions are consistently reduced by lowering equivalence ratio for both types. For Type 5, as CO_2 content in the gas increases to 34%, the NOx reduction trend is obvious.

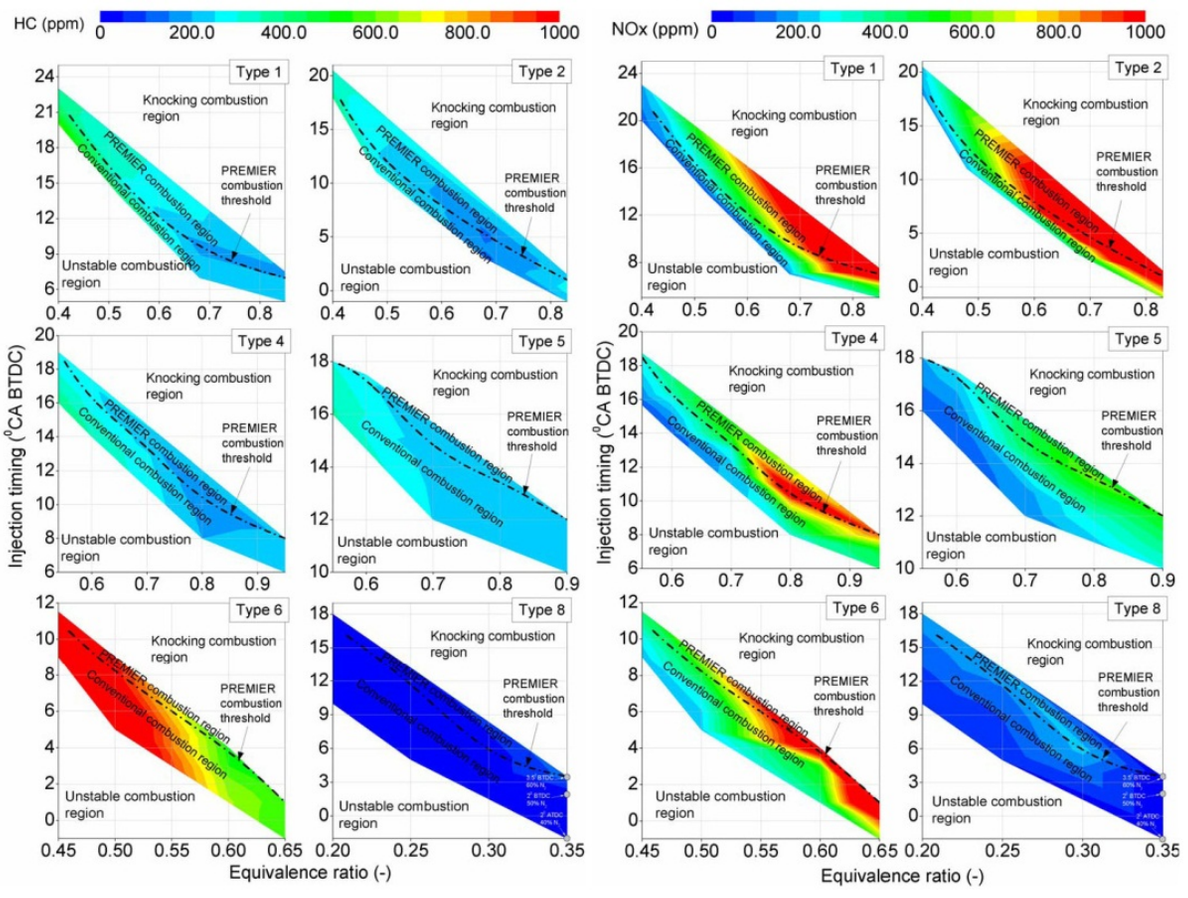

Figure 21. Experimental mapping of HC and NOx distribution

The opposite trend is observed for Type 6, as shown in Figure 20. This type of gas has very high content of H_2-56.8%, and very low content of CO_2-2.2%. For the limited range of equivalence ratios and injection timings, the PREMIER combustion region is very narrow, and at even higher equivalence ratios, the stable combustion will easily turn to knocking. These results show that in order to achieve PREMIER combustion with the best case scenario in terms of efficiency and emissions the equivalence ratio and injection timing should be maintained within certain range, depending on H_2 and CO_2 fractions in syngas. Figure 21 shows that for Type 6 the NOx emissions can be compared with those of Type 2. Even with the retarding of the injection timing closer to TDC, NOx emissions level is still comparably high. On the other hand, CO emissions are significantly reduced.

In addition, the performance and emissions of pilot-ignited dual-fuel engine operated on 100% H_2 as a primary fuel was investigated, shown as Type 8. The data at equivalence ratios of 0.2, 0.25 and 0.3 are related to the engine operation without dilution. Further increase in

equivalence ratio above 0.3 caused knocking combustion. To further increase the energy supply from hydrogen the equivalence ratio of 0.35 was used with the 40%, 50% and 60% of N_2 dilution. Previous research suggests that NOx emissions in hydrogen-fueled engines can be reduced by using EGR or using the nitrogen dilution [44, 45]. These studies reported that NOx emissions were reduced by the reduction in peak combustion temperature due to the presence of diluent gas. Mathur *et al.* [45] showed that with larger concentrations of nitrogen as diluent, a greater amount of combustion heat can be absorbed, which results in reducing peak flame temperature and NOx. IMEP increases with the equivalence ratio. For the equivalence ratios of 0.2 and 0.25, the minimum advanced injection timing for the maximum IMEP was obtained at 17° BTDC and 12° BTDC, respectively. At these injection timings PREMIER combustion occurs. For the case with N_2 dilution, injection timing has greater effect on IMEP than the dilution rate. IMEP gradually increased as the injection timing was advanced along with the increased amount of diluent from 40% to 60%. Due to low equivalence ratios, very low level of NOx was detected without N_2 dilution. At the conditions with N_2 dilution the NOx showed further decrease. For the conditions without dilution, CO and HC emissions were significantly reduced to the level of about 6 ppm and 20 ppm, respectively. However, for the conditions with N_2 dilution CO varied from min.-15 ppm to max.-891 ppm and HC varied from min.-20 ppm to max.-125 ppm.

6. Conclusion

The new PREMIER combustion mode in a dual-fuel engine fuelled with natural gas, syngas and hydrogen was investigated via engine experiments. The following conclusions can be drawn from this research:

- PREMIER combustion combines two main stages of heat release, the first is gaseous fuel flame propagation and the second is end-gas mixture auto-ignition. The second stage can be mainly controlled by the pilot fuel injection timing, gaseous fuel equivalence ratio, and EGR rate. The delay time for mixture autoignition in the end-gas region is defined as the time from early kernel development to the transition point where slower combustion rate (flame propagation) is changed to faster combustion rate (autoignition). It was found that the rate of maximum pressure rise increases as the second stage ignition delay decreases. PREMIER combustion was observed for natural gas and all syngas types investigated in this paper. This type of combustion can enhance the engine performance and increase the efficiency.
- In both PREMIER and knocking combustion with natural gas, moderate and high intensities of OH* radicals were detected, respectively, at wavelengths of 286 and 310 nm when the flame front reached the optical sensor location region. In knocking combustion, the OH* radical emission intensities were stronger than those in PREMIER combustion, and in conventional combustion, these emission intensities could barely be detected. PREMIER combustion differs from knocking combustion in terms of size, gradients, and spatial distribution of exothermic centers in the end-gas region. High-frequency oscillation of the in-cylinder pressure did not occur during the PREMIER combustion mode with natural gas.

- An increase in the fuel mass fraction burned in the second stage of heat release affects the rate of maximum pressure rise. When hydrogen content in syngas is increased the same rate of maximum pressure rise can be achieved with lower amount of fuel mass fraction burned during the second stage, meaning that the increased amount of hydrogen in syngas induces an increase in the mean combustion temperature, IMEP and efficiency, but also a significant increase in NOx emissions. The results also show that when CO_2 content in the gas reaches 34%, the rate of maximum pressure rise, as well as, the mean combustion temperature, IMEP, thermal efficiency and NOx decrease despite the increase in fuel mass fraction burned during the second stage of heat release rate.
- For pure hydrogen at equivalence ratios of 0.2, 0.25 and 0.3 without dilution, very low CO and HC emissions were detected. The further increase in equivalence ratio above 0.3 led to knocking combustion. At the equivalence ratio of 0.35 with N_2 dilution, NOx level significantly decreased but CO level increased.

Author details

Ulugbek Azimov*
Department of Mechanical Engineering,Curtin University, Malaysia campus

Eiji Tomita and Nobuyuki Kawahara
Department of Mechanical Engineering, Okayama University, Japan

7. References

[1] Weaver CS. Natural gas vehicles – a review of the state of the art, SAE Paper, 892133.
[2] Nichols RJ. The challenges of change in the auto industry: Why alternative fuels? J Eng Gas Turb Power 1994;116:727-32.
[3] Lieuwen T, Yang V, Yetter R. Synthesis gas combustion: Fundamentals and applications. Taylor & Francis Group 2010.
[4] Shilling NZ, Lee DT. IGCC-Clean power generation alternative for solid fuels: GE Power Systems. PowerGenAsia 2003.
[5] Bade Shrestha SO, Karim GA. Hydrogen as an additive to methane for spark ignition engine applications. Int J Hydrogen Energy 1999;24:577-86.
[6] Stebar RF, Parks FB. Emission control with lean operation using hydrogen-supplimented fuel. SAE Paper 740187.
[7] Jingding L, Linsong G, Tianshen D. Formation and restraint of toxic emissions in hydrogen-gasoline mixture fueled engines. Int J Hydrogen Energy 1998;23:971-75.
[8] Pushp M, Mande S. development of 100% producer gas engine and field testing with pid governor mechanism for variable load operation. SAE Paper 2008-28-0035.

* Corresponding Author

[9] Yamasaki Y, Tomatsu G, Nagata Y, Kaneko S. Development of a small size gas engine system with biomass gas (combustion characteristics of the wood chip pyrolysis gas), SAE Paper 2007-01-3612.
[10] Ando Y, Yoshikawa K, Beck M, Endo H. Research and development of a low-BTU gas-driven engine for waste gasification and power generation. Energy 2005;30:2206-18.
[11] McTaggart-Cowan GP, Jones HL, Rogak SN, Bushe WK, Hill PG, Munshi SR. The effect of high-pressure injection on a compression-ignition, direct injection of natural gas engine. J Eng Gas Turb Power 2007;129: 579-88.
[12] Su W, Lin Z. A study on the determination of the amount of pilot injection and rich and lean boundaries of the pre-mixed CNG/Air mixture for a CNG/Diesel dual-fuel engine. SAE paper, 2003-01-0765.
[13] Tomita E, Fukatani N, Kawahara N, Maruyama K, Komoda T. Combustion characteristics and performance of supercharged pyrolysis gas engine with micro-pilot ignition. CIMAC congress 2007. Paper No. 178.
[14] Liu Z, Karim GA. Simulation of combustion processes in gas-fuelled diesel engine. J Power Energy 1997;211:159-69.
[15] Ma F, Wang Y, Ding S, Jiang L. Twenty percent hydrogen-enriched natural gas transient performance research. Int J Hydrogen Energy 2009;34:6423-31.
[16] Sung CJ, Law CK. Fundamental combustion properties of H2/CO mixtures: Ignition and flame propagation at elevated temperatures. Combust Sci.Tech. 2008;180:1097-1116.
[17] Heywood JB. Internal combustion engine fundamentals. New-York: McGraw-Hill 1988.
[18] Nakagawa Y, Takagi Y, Itoh T, and Iijima T. Laser shadowgraphic analysis of knocking in SI engine. SAE Paper, 845001.
[19] Pan J, Sheppard CGW, Tindall A, Berzins M, Pennington SV and Ware JM. End-gas inhomogeneity, autoignition and knock. SAE Paper, 982616.
[20] Kawahara N, Tomita E, and Sakata Y. Auto-ignited kernels during knocking combustion in a spark-ignition engine. Proc. Combust. Inst. 2007;31:2999-3006.
[21] Bauerle B, Hoffman F, Behrendt F, and Warnatz J. Detection of hot spots in the end gas of an internal combustion engine using two-dimensional LIF of formaldehyde. In: 25th Symposium (Int.) on Combustion 1994;25:135-141.
[22] Stiebels B, Schreiber M, and Sadat Sakak A. Development of a new measurement technique for the investigation of end-gas autoignition and engine knock. SAE Paper, 960827.
[23] Pan J, and Sheppard CGW. A theoretical and experimental study of the modes of end gas autoignition leading to knock in SI engines. SAE Paper, 942060.
[24] Li J, Zhao H, Ladommatos N. Research and development of controlled auto-ignition (CAI) combustion in a 4-stroke multi cylinder gasoline engine. SAE Paper, 2001-01-3608.
[25] Santoso H, Matthews J, Cheng WK. Managing SI/HCCI dual-mode engine operation. SAE Paper, 2005-01-0162.

[26] Persson H, Hultqvist A, Johansson B, Remon A. Investigation of the early flame development in spark assisted HCCI combustion using high-speed chemiluminescence imaging. SAE Paper, 2007-01-0212.

[27] Ma F, Wang J, Wang Yu, Wang Y, Li Y, Liu H, Ding S. Influence of different volume percent hydrogen/natural gas mixtures on idle performance of a CNG engine. Energy & Fuels 2008;22:1880-87.

[28] Higgin RMR, Williams A. A shock-tube investigation of the ignition of lean methane and n-butane mixtures with oxygen. In: Symposium (Int.) on Combustion 1969;12:579-90.

[29] Zellner R, Niemitz KJ, Warnatz J, Gardiner Jr WC, Eubank CS, Simmie JM. Hydrocarbon induced acceleration of methane-air ignition. Prog Astronaut Aeronaut 1981;88:252-72.

[30] Eubank CS, Rabinovitz MJ, Gardiner Jr WC, Zellner RE. Shock-initiated ignition of natural gas-air mixtures. In: 18th Symposium (Int.) on Combustion 1981;18:1767-74.

[31] Crossley RW, Dorko EA, Scheller K, Burcat A. The effect of higher alkanes on the ignition of methane-oxygen-argon mixtures in shock waves. Comb. Flame 1972;19:373-78.

[32] Westbrook CK, Pitz WJ, Leppard WR. The autoignition chemistry of paraffinic fuels and pro-knock and anti-knock additives: a detailed chemical kinetic study. SAE Paper, 912314.

[33] Jun D, Ishii K, Iida N. Autoignition and combustion of natural gas in a 4-stroke HCCI engine. JSME International J. 2003;46:60-67.

[34] Saito H, Sakurai T, Sakonji T, Hirashima T, Kanno K. Study on lean-burn gas engine using pilot oil as the ignition source. SAE Paper, 2001-01-0143.

[35] Azimov U, Tomita E, Kawahara N, Harada Y. PREMIER (Premixed Mixture Ignition in the End-gas Region) combustion in a natural gas dual-fuel engine: Operating range and exhaust emissions. Int J Engine Research 2011;12:484-497.

[36] Itoh T, Nakada T, and Takagi Y. Emission characteristics of OH and C2 radicals under engine knocking. JSME International J. 1995;38:230-237.

[37] Hashimoto S, Amino Y, Yoshida K, Shoji H and Saima A. Analysis of OH radical emission intensity during autoignition in a 2-stroke SI engine. In: Proceedings of the 4th COMODIA 1998, 405-410.

[38] Gaydon AG. The spectroscopy of flames, 2nd edition, 1974 (Chapman and Hall Ltd, London).

[39] Itoh T, Takagi T, and Iijima T. Characteristics of mixture fraction burned with autoignition and knocking intensity in a spark ignition engine. Trans. Japan Soc. Mech. Eng. 1985;52:3068.

[40] Coats CM, and Williams A. Investigation of the ignition and combustion of n-Heptane-oxygen mixtures. Proc. Combust. Institute 1979;17:611-621.

[41] Zhao H, and Ladommatos N. Optical diagnostics for soot and temperature measurement in diesel engines. Prog. Energy Combust. Sci. 1998;24:221-255.

[42] Vattulainen J. Experimental determination of spontaneous diesel flame emission spectra in a large diesel engine operated with different diesel fuel qualities. SAE Paper, 981380.
[43] Incropera FP and DeWitt DP. Fundamentals of heat and mass transfer, 4th edition, 1996 (John Wiley & Sons).
[44] Bose PK, Maji D. An experimental investigation on engine performance and emissions of a single cylinder diesel engine using hydrogen as induced fuel and diesel as injected fuel with exhaust gas recirculation. Int J Hydrogen Energy 2009;34:4847-54.
[45] Mathur HB, Das LM, Patro TN. Hydrogen-fuelled diesel engine: Performance improvement through charge dilution techniques. Int J Hydrogen Energy 1993;18:421-31.